# Supporting Information

## 1 Meshing Scheme for Simulations

For simulating the evolution of filament shapes (Eqs. 1.2, 1.5 in paper, with results shown in Fig. 1, 2 of the paper) a dynamical remeshing scheme was used. The total number of grid points along each filament is $N = 800$. This number does not change from one time step to another. However, the points are dynamically moved to the parts of the filament where higher resolution is required (determined by considering the inter-filament separation distance and the curvature), mainly the tip. Below, we plot the filaments using just the gird points without any interpolation at the last time step of our simulation. As evident, the points are not equally spaced, in fact they are closely bunched at the tip. We define quantity $ds$ as the separation distance of two neighboring gird points. $ds$ is plotted below for each of the 800 points, for the same time-steps as Fig. 1 of the paper. The separation distance at the tip ($N = 400$) has decreased by five orders of magnitude. This equals the change in the minimum separation distance of the two filaments and the increase in the curvature at the tip. As time advances, the separation distance of more grid points matches the minimum separation distance. Towards the last time steps, roughly 200 of the points, or 25% of our numerical resolution is bunched at the tip, an infinitesimal length along the filament, to properly resolve the singularity.

## 2 Solving the Similarity ODE under Local Approximation

### 2.1 Self-Similar Form

The vortex filament $i$ is described by $r_i(s_i, t)$, where $r_i$ is the filament position parametrized by arc length parameter $s_i$ and time $t$. We assume that close to the singularity, a similarity solution exists of the form,

$$r_i(s, t) = l_i(t)G(s/l_i(t)), \tag{1}$$

where the only relevant length scale is $l_i(t) = \sqrt{|\Gamma_i|(t^* - t)}$.

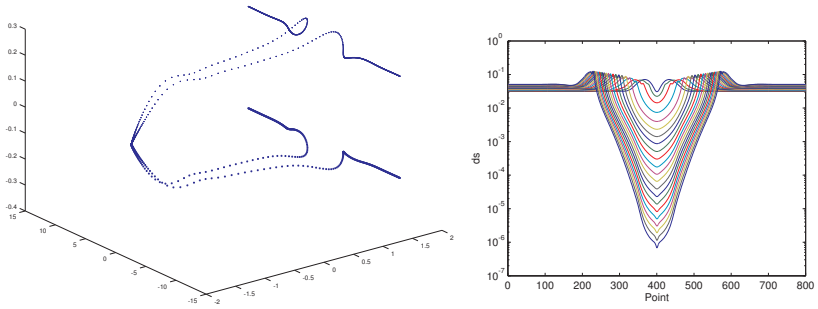


Figure 1: Left: Curves in Fig. 1 of the paper but with the points used in the last time step ($1 - t^*/t = 1.2 \times 10^{-10}$) explicitly shown. The points are closer together near the tip where a higher resolution is required. The separation distance between points at the tip keeps up with the vanishing separation distance between the filaments to ensure numerical accuracy. Right: Separation distance for the grid points used in numerically approximating curves of Fig. 1 of the paper as a function of point number for different time steps. Many more points are pushed towards the tip (where the separation distance is least) to maintain the required numerical resolution.

## 2.2 PDE of Motion

Under local approximation the velocity induced at point $R$ by a vortex filament is

$$v_{ext}(R) = -\frac{\Gamma}{2\pi}\frac{(R - r(s)) \times r'(s)}{|R - r(s)|^2}, \tag{2}$$

where $r(s)$ is the closest point on the filament to point $R$. For well-behaved geometries, this is equivalent to

$$\frac{d|R - r(s)|}{ds} = 0. \tag{3}$$

The self-induced velocity is given by,

$$v_{self}(r) = -\frac{\Gamma}{4\pi}\kappa \ln\left(\frac{r_c}{\sigma}\right) b, \tag{4}$$

where $\kappa$ is the curvature, $r_c$ radius of curvature, $\sigma$ diameter of the filament, and $b$ the binormal vector.

## 2.3 Delayed ODE for Similarity Solution

Consider the self-similar time-independent form of two vortex filaments.

We use arc length parameter $\eta$ to move along the two filaments. We define two other arc length parameters $\eta_1$ and $\eta_2$ to designate the nearest point on the other filament. This means on filament 1, $G_1(\eta)$ is closest to $G_2(\eta_2)$; and on filament 2, $G_2(\eta)$ is closest to $G_1(\eta_1)$. Equivalently,

$$\frac{d}{d\eta_2}|\sqrt{|\Gamma_2|}G_2(\eta_2) - \sqrt{|\Gamma_1|}G_1(\eta)|^2 = 0. \tag{5}$$

For well behaved geometries (and fixed $\eta$), this is equivalent to,

$$\sqrt{|\Gamma_2|}G_2'(\eta_2) \cdot (\sqrt{|\Gamma_2|}G_2(\eta_2) - \sqrt{|\Gamma_1|}G_1(\eta)) = 0. \tag{6}$$

The line connecting a point on filament 1 to the nearest point on filament 2 should be perpendicular to the tangential component of filament 2 at that point. $\eta_2$ is clearly a function of $\eta$. Its differential dependence on $\eta$ is given by,

$$\boxed{\frac{d\eta_2}{d\eta} = \frac{\sqrt{|\Gamma_1|}G_2'(\eta_2) \cdot G_1'(\eta)}{G_2''(\eta_2) \cdot \left(\sqrt{|\Gamma_2|}G_2(\eta_2) - \sqrt{|\Gamma_1|}G_1(\eta)\right) + \sqrt{|\Gamma_2|}|G_2'(\eta_2)|^2}} \tag{7}$$

Similarly $\eta_1$ is related to $\eta$,

$$\boxed{\frac{d\eta_1}{d\eta} = \frac{\sqrt{|\Gamma_2|}G_1'(\eta_1) \cdot G_2'(\eta)}{G_1''(\eta_1) \cdot \left(\sqrt{|\Gamma_1|}G_1(\eta_1) - \sqrt{|\Gamma_2|}G_2(\eta)\right) + \sqrt{|\Gamma_1|}|G_1'(\eta_1)|^2}} \tag{8}$$

We define $\alpha_i = \frac{1}{2\pi}\ln\left(\frac{r_c^i}{\sigma_i}\right)$.

The equation of motion for filament 1 becomes,

$$G_1(\eta) - \eta G_1'(\eta) = \alpha\frac{\Gamma_1}{|\Gamma_1|}G_1'(\eta)\times G_1''(\eta) + \frac{\Gamma_2}{\pi\sqrt{|\Gamma_1|}}\frac{\left(\sqrt{|\Gamma_1|}G_1(\eta) - \sqrt{|\Gamma_2|}G_2(\eta_2)\right)\times G_2'(\eta_2)}{|\sqrt{|\Gamma_1|}G_1(\eta) - \sqrt{|\Gamma_2|}G_2(\eta_2)|^2}. \tag{9}$$

Crossing the above expression with $G'$ and using the fact that $G'\times G'\times G'' = G'(G'.G'') - G''(G'.G') = -G''$ –since $G'$ is normalized, yields,

$$G_1''(\eta) = -\frac{|\Gamma_1|}{\alpha_1\Gamma_1}G_1'(\eta)\times\left(G_1(\eta) - \frac{\Gamma_2}{\pi\sqrt{|\Gamma_1|}}\frac{\left(\sqrt{|\Gamma_1|}G_1(\eta) - \sqrt{|\Gamma_2|}G_2(\eta_2)\right)\times G_2'(\eta_2)}{|\sqrt{|\Gamma_1|}G_1(\eta) - \sqrt{|\Gamma_2|}G_2(\eta_2)|^2}\right). \tag{10}$$

Equations 7 and 8 require $G''$ to evaluate the nearest point on the opposing filament. Hence, to have a closed set of ordinary differential equations, we need to go one order higher. $G''$ will then become an input which is used to evaluate $G'''$. This also adds two new vectors ($G_1''$ and $G_2''$ at the start point) to the

initial conditions. Differentiating the last equation with respect to $\eta$ gives,

$$\boxed{\begin{aligned} G_1'''(\eta) = &-\frac{|\Gamma_1|}{\alpha_1\Gamma_1}G_1''(\eta)\times\left(G_1(\eta)-\frac{\Gamma_2}{\pi\sqrt{|\Gamma_1|}}\frac{\left(\sqrt{|\Gamma_1|}G_1(\eta)-\sqrt{|\Gamma_2|}G_2(\eta_2)\right)\times G_2'(\eta_2)}{|\sqrt{|\Gamma_1|}G_1(\eta)-\sqrt{|\Gamma_2|}G_2(\eta_2)|^2}\right)\\ &-\frac{|\Gamma_1|}{\alpha_1\Gamma_1}G_1'(\eta)\times\left(G_1'(\eta)-\frac{\Gamma_2}{\pi\sqrt{|\Gamma_1|}}\frac{\left(\sqrt{|\Gamma_1|}G_1'(\eta)-\sqrt{|\Gamma_2|}G_2'(\eta_2)\frac{d\eta_2}{d\eta}\right)\times G_2'(\eta_2)}{|\sqrt{|\Gamma_1|}G_1(\eta)-\sqrt{|\Gamma_2|}G_2(\eta_2)|^2}\right.\\ &\qquad-\frac{\Gamma_2}{\pi\sqrt{|\Gamma_1|}}\frac{\left(\sqrt{|\Gamma_1|}G_1(\eta)-\sqrt{|\Gamma_2|}G_2(\eta_2)\right)\times G_2''(\eta_2)\frac{d\eta_2}{d\eta}}{|\sqrt{|\Gamma_1|}G_1(\eta)-\sqrt{|\Gamma_2|}G_2(\eta_2)|^2}\\ &\qquad+\frac{\Gamma_2}{\pi\sqrt{|\Gamma_1|}}\frac{\left(\sqrt{|\Gamma_1|}G_1(\eta)-\sqrt{|\Gamma_2|}G_2(\eta_2)\right)\times G_2'(\eta_2)}{|\sqrt{|\Gamma_1|}G_1(\eta)-\sqrt{|\Gamma_2|}G_2(\eta_2)|^4}\\ &\left.\left(\sqrt{|\Gamma_1|}G_1'(\eta)-\sqrt{|\Gamma_2|}G_2'(\eta_2)\frac{d\eta_2}{d\eta}\right)\cdot\left(\sqrt{|\Gamma_1|}G_1(\eta)-\sqrt{|\Gamma_2|}G_2(\eta_2)\right)\right) \end{aligned}} \tag{11}$$

Similarly, for filament 2 we have,

$$G_2''(\eta) = -\frac{|\Gamma_2|}{\alpha_2\Gamma_2}G_2'(\eta)\times\left(G_2(\eta)-\frac{\Gamma_1}{\pi\sqrt{|\Gamma_2|}}\frac{\left(\sqrt{|\Gamma_2|}G_2(\eta)-\sqrt{|\Gamma_1|}G_1(\eta_1)\right)\times G_1'(\eta_1)}{|\sqrt{|\Gamma_2|}G_2(\eta)-\sqrt{|\Gamma_1|}G_1(\eta_1)|^2}\right). \tag{12}$$

And in higher order,

$$\boxed{\begin{aligned} G_2'''(\eta) = &-\frac{|\Gamma_2|}{\alpha_2\Gamma_2}G_2''(\eta)\times\left(G_2(\eta)-\frac{\Gamma_1}{\pi\sqrt{|\Gamma_2|}}\frac{\left(\sqrt{|\Gamma_2|}G_2(\eta)-\sqrt{|\Gamma_1|}G_1(\eta_1)\right)\times G_1'(\eta_1)}{|\sqrt{|\Gamma_2|}G_2(\eta)-\sqrt{|\Gamma_1|}G_1(\eta_1)|^2}\right)\\ &-\frac{|\Gamma_2|}{\alpha_2\Gamma_2}G_2'(\eta)\times\left(G_2'(\eta)-\frac{\Gamma_1}{\pi\sqrt{|\Gamma_2|}}\frac{\left(\sqrt{|\Gamma_2|}G_2'(\eta)-\sqrt{|\Gamma_1|}G_1'(\eta_1)\frac{d\eta_1}{d\eta}\right)\times G_1'(\eta_1)}{|\sqrt{|\Gamma_2|}G_2(\eta)-\sqrt{|\Gamma_1|}G_1(\eta_1)|^2}\right.\\ &\qquad-\frac{\Gamma_1}{\pi\sqrt{|\Gamma_2|}}\frac{\left(\sqrt{|\Gamma_2|}G_2(\eta)-\sqrt{|\Gamma_1|}G_1(\eta_1)\right)\times G_1''(\eta_1)\frac{d\eta_1}{d\eta}}{|\sqrt{|\Gamma_2|}G_2(\eta)-\sqrt{|\Gamma_1|}G_1(\eta_1)|^2}\\ &\qquad+\frac{\Gamma_1}{\pi\sqrt{|\Gamma_2|}}\frac{\left(\sqrt{|\Gamma_2|}G_2(\eta)-\sqrt{|\Gamma_1|}G_1(\eta_1)\right)\times G_1'(\eta_1)}{|\sqrt{|\Gamma_2|}G_2(\eta)-\sqrt{|\Gamma_1|}G_1(\eta_1)|^4}\\ &\left.\left(\sqrt{|\Gamma_2|}G_2'(\eta)-\sqrt{|\Gamma_1|}G_1'(\eta_1)\frac{d\eta_1}{d\eta}\right)\cdot\left(\sqrt{|\Gamma_2|}G_2(\eta)-\sqrt{|\Gamma_1|}G_1(\eta_1)\right)\right) \end{aligned}} \tag{13}$$

The four boxed equations above are a set of coupled ODEs in 20 variables. The initial conditions specify at the start point $G_1$, $G_2$, $G_1'$, $G_2'$, from which $G_1''$, and $G_2''$ are computed; in addition, $\eta_1(0) = 0$ and $\eta_2(0) = 0$. The equations are then solved numerically.

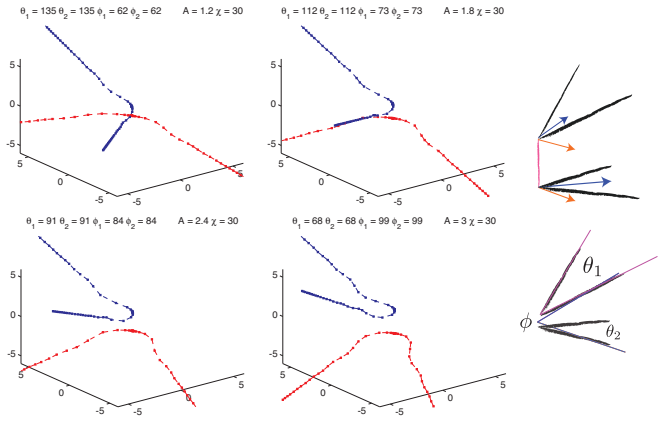


Figure 2: Non-universality of the similarity solutions. Here the $G'$ vectors of the two filaments (part of the initial conditions in similarity space) are skewed by $2\chi = 60$ degrees. The separation distance between the two filaments in the similarity space $A$ is varied for each plot. The shapes are characterized by four angles of the 'tent'. Clearly, the 'tent' geometry is not universal, but dependent on the initial conditions.

# 3 Non-universality of Similarity Solutions

To demonstrate that the solutions to the similarity ODE are non-universal, but dependent on the initial conditions in similarity space, we have solved the similarity ODE for different separation distances between the starting points $A = |G_1(0) - G_2(0)|$. In real space $A$ corresponds to the numerical pre factor for the scaling law in the limit of approaching the singularity. In each case the coplanar vectors $G_1'(0)$ and $G_2'(0)$ form an angle of 60 degrees. The circulations are equal in magnitude.

The shape of the solution is quantified using the geometry of the resulting 'tent', as characterized by the opening angles $\theta_{1,2}$ and $\phi_{1,2}$ (see Fig. 2). The filaments are no longer symmetric and many different 'tent' geometries are possible. This is an explicit demonstration of the asymptotic geometry not being universal.